Journal of Molecular Liquids 435 (2025) 128162

Contents lists available at ScienceDirect

Journal of Molecular Liquids

journal homepage: www.elsevier.com/locate/molliq

Cobalt(II) complex formation with nitrate and chloride anions in the [C_4mim][Tf_2N] ionic liquid

Martina Sanadar [a,b], Anđela Kovačević [b], José Alejandro Ricardo García [b], Marilena Tolazzi [b], Andrea Melchior [b,*]

[a] Centre de Biophysique Moléculaire, CNRS UPR 4301 Université d'Orléans, rue Charles Sadron, 45071 Orléans, France
[b] Dipartimento Politecnico, Università di Udine, Laboratorio di Tecnologie Chimiche, via del Cotonificio 108, 33100 Udine, Italy

ARTICLE INFO

Keywords:
Ionic liquids
Cobalt
Thermodynamics
Coordination
Molecular dynamics simulations
Calorimetry
Speciation

ABSTRACT

This study investigates the coordination chemistry and thermodynamics of cobalt(II) complex formation with nitrate (NO_3^-) and chloride (Cl^-) anions in the dry ionic liquid [C_4mim][Tf_2N]. Using UV–visible spectrophotometry, isothermal titration calorimetry (ITC), density functional theory (DFT) calculations, and molecular dynamics (MD) simulations, we elucidate the stability, structure, and energetics of the formed complexes. Spectroscopic and computational results reveal that cobalt(II) maintains octahedral coordination with nitrate, forming stepwise 1:1, 1:2, and 1:3 complexes, with a progressive displacement of $[Tf_2N]^-$ anions. In contrast, chloride coordination induces a transition from octahedral (1:1) to a mixed tetrahedral/penta-coordinated (1:2) geometry, ultimately stabilizing tetrahedral 1:3 and 1:4 species. Thermodynamic analysis highlights the central role of solvation effects and ionic liquid restructuring in determining complex stability. These findings enhance the comprehension of cobalt coordination in Tf_2N-based ionic liquids and constitute a contribution to the understanding of fundamental phenomena with implications for metal recovery.

1. Introduction

The coordination chemistry of metal ions in ionic liquids (ILs) have attracted much attention in the last two decades, due to the numerous applications such as metal extractions and selective separations in hydrometallurgical processes for selective extractions of transition metals [1–6] and *f*-block elements [7,8], electrodepositions [9–12], energy storage [13–15] and catalysis [16,17]. ILs are salts composed of bulky organic cations and inorganic/organometallic anions existing in the liquid state at temperatures < 100 °C (also called Room Temperature ILs when liquid at 25 °C). The origin of such low melting temperatures has been traditionally assigned to a low enthalpy of melting due to the low lattice energy originating from the weakening of coulombic interaction caused by charge delocalization and bulkiness of the ions [18,19]. Nevertheless, recently the entropy of fusion has also been proposed to be the main reason for their low melting point [20]. RTILs are attractive for many applications as alternatives to classical organic solvents for the applications mentioned above owing to numerous interesting features: negligible vapor pressure, non-flammability, excellent electric conductivity, high thermal and electrochemical stabilities, and good solvation ability for both charged and neutral species [17]. They also display a strong correlation between their structure and physical-chemical properties, thus specific RTILs can be designed for optimal performances in given tasks. It should be recalled that these attractive advantages over organic solvents are balanced by their high cost, the synthetic process, high viscosity, and their toxicity, which initially was considered negligible due to their low vapor pressure [21]. However, recent works are precisely aimed at addressing the sustainability and biocompatibility of ILs to take full advantage of them [22].

Contrary to the case of organic solvents [23–28], the study of coordination and thermodynamics of metal complex formation in RTILs have received much less attention [29–32], despite the knowledge that species distribution in solution is key information to understand the molecular processes at the basis of the applications involving dissolved metal ions [33–35]. Most of the thermodynamic studies available have been done for lanthanide and actinide complexation with small inorganic ligands (*e.g.*, Cl^-, NO_3^-) and organic ligands employed in liquid-liquid extractions (some examples in refs. [36–39]). As for the transition metals, several studies were carried out in RTILs containing the weakly coordinating bis(trifluoromethylsulfonyl)imide $[Tf_2N]^-$ anion

* Corresponding author.
E-mail address: andrea.melchior@uniud.it (A. Melchior).

https://doi.org/10.1016/j.molliq.2025.128162
Received 28 March 2025; Received in revised form 12 July 2025; Accepted 14 July 2025
Available online 16 July 2025

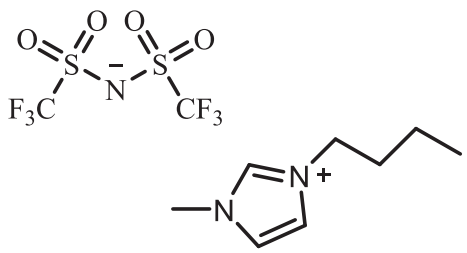

Scheme 1. 1-butyl-3-methylimidazolium bis(trifluoromethylsulfonyl)imide.

[29,40] which have been employed for sensing, depositions, and separative applications [41,42].

Recently, the Co(II), Ni(II) and Zn(II) solvation in $[C_4mim][Tf_2N]$ (1-butyl-3-methylimidazolium bis(trifluoromethylsulfonyl)imide, Scheme 1) has been defined using X-ray absorption, and theoretical methods [43–45], showing that these bivalent metals exist as $[M(Tf_2N)_6]^{4-}$ species where the 6 $[Tf_2N]^-$ anions coordinate through the -SO_2 oxygens in a mono-dentate mode (Scheme S1).

In contrast with other coordination modes proposed in previous studies in solution [46,47] and in the solid state [48], and with what was found for metals with larger ionic radii (*e.g.* lanthanides [8]), in the above-mentioned works, it was unambiguously shown that bidentate coordination of $[Tf_2N]^-$ was not present in solution. This result was explained by admitting that the conformational rigidity of the anion prevents the monodentate coordination mode in solution with such small ions [44].

Co(II) speciation in $[Tf_2N]^-$-containing RTILs is particularly interesting for some applications such as electrodepositions [49–54] and separations [4]. In recent years, numerous studies focused on the development of RTILs-based hydrometallurgical processes aimed at recycling this "critical raw material" [55] from end-of-life devices such as Li-ion batteries or permanent magnets [56] as well as its separation from radioactive waste [57]. Moreover, Co(II) solutions in $[Tf_2N]^-$-containing RTILs were shown to have peculiar properties such as thermochromism [58,59] and thermotropism [48].

In this work, the Co(II) complex formation with nitrate (NO_3^-) and chloride (Cl^-) ions in $[C_4mim][Tf_2N]$ is studied by means of spectrophotometry and isothermal titration calorimetry (ITC). Density functional theory (DFT) and molecular dynamics (MD) simulations have been employed to obtain structural information on the species formed at the molecular level. Previous studies have highlighted that the interaction of these anions with transition metal species can significantly influence solubility, coordination environment, and redox behavior [5,29,50,60–62]. In particular, two anions are often present in electrochemical processes for cobalt recovery and thin film electrodeposition, where the metal speciation plays a crucial role in determining the conditions, type, and morphology of the obtained metal [49–54].

2. Materials and methods

2.1. Chemicals

$[C_4mim][Tf_2N]$ IL (Iolitec, 99.5 %), cobalt (II) bis(trifluoromethanesulfonyl)imide salt ($Co(Tf_2N)_2$, Alfa Aesar, >98 %), 1-Butyl-3-methylimidazolium nitrate ($[C_4mim][NO_3]$, Iolitec, >98 %) and 1-Butyl-3-methylimidazolium chloride ($[C_4mim][Cl]$, Iolitec, >99 %) were used without further purification. The highly $[C_4mim][Tf_2N]$, $[C_4mim][NO_3]$ and $[C_4mim][Cl]$ were dried under vacuum for at least 48 h at 70 °C. The salt $Co(Tf_2N)_2$ was dried under vacuum without heating. All the starting solutions were stored under N_2 atmosphere in a dry-box (H_2O < 1 ppm). Water content in the $[C_4mim][Tf_2N]$ employed to prepare the solutions was checked by Karl Fischer titration (<100 ppm).

2.2. Spectrophotometric titrations

The formation constants (β_j) for the equilibrium (1) can be treated as for the Co + jX ⇄ $[Co(X)_j]$ equation where the charges are omitted:

$$\beta_j = \frac{[CoX_j]}{[Co][X]^j} \quad (1)$$

The Gibbs free energy change associated is calculated as: $\Delta G_{\beta j} = -RT\ln\beta_j$.

Table 1
Overall (log β_j) and Stepwise (log K_j) Stability Constants and Thermodynamic Parameters (kJ mol^{-1}) relative to the reaction $Co(II) + jNO_3^- \leftrightarrows [Co(NO_3)_j]^{2-j}$ in $[C_4mim][Tf_2N]$ ($T = 298.15$ K). Standard deviations are reported in parentheses.

j	log β_j	$\Delta G_{\beta j}$	$\Delta H_{\beta j}$	$T\Delta S_{\beta j}$	log K_j	ΔG_{Kj}	ΔH_{Kj}	$T\Delta S_{Kj}$
1	4.87 (8)	−27.8	−14.4 (4)	13.4	4.87	−27.8	−14.4	13.4
2	8.1(1)	−46.2	−22.4 (4)	23.8	3.23	−18.4	−8.0	10.4
3	10.4 (3)	−59.3	−36.7 (5)	22.6	2.3	−13.1	−14.3	−1.2

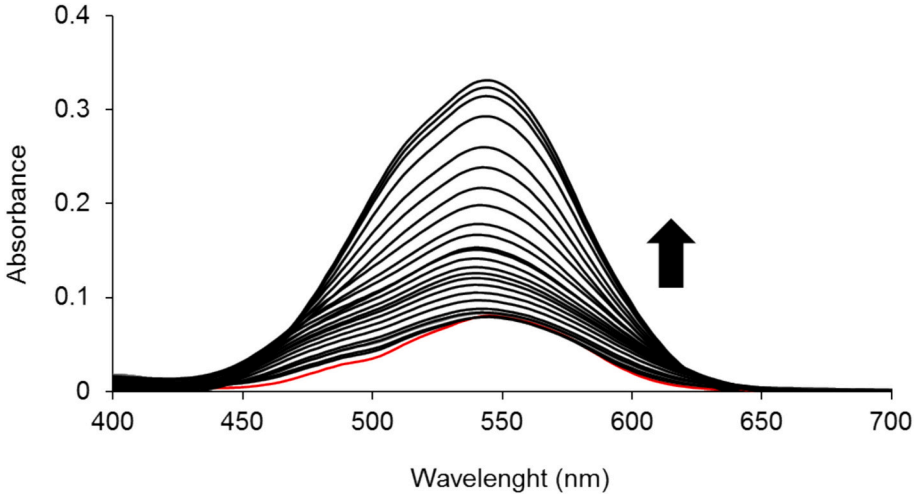

Fig. 1. Spectrophotometric titration of Co(II) with NO_3^- in dry $[C_4mim][Tf_2N]$ at 298 K. Initial solution: $V_0 = 1.83$ mL and $C_{Co} = 3$ mM. Titrant solution: $C_L = 82.6$ mM. Final $R_L = 4.35$. The black arrow shows the direction of spectra evolution.

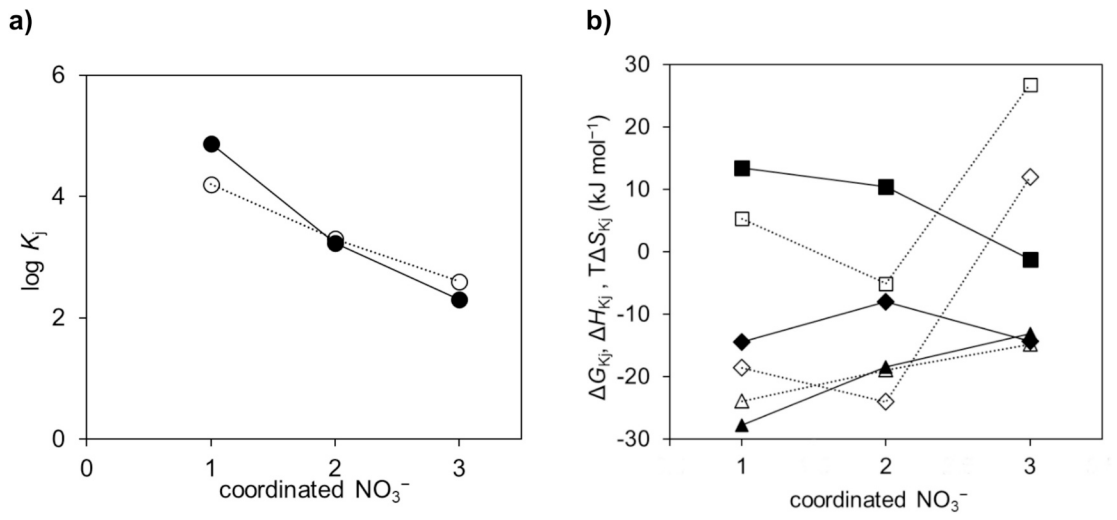

Fig. 2. (a) Stepwise stability constants (log K_j) for the formation of $M(NO_3)_j$ species (M = Co, Ni) *vs.* the number of coordinated NO_3^- anions. (b) Stepwise thermodynamic parameters ΔG_{Kj} (triangles) ΔH_{Kj} (diamonds) and $T\Delta S_{Kj}$ (squares) plotted as a function of the number of coordinated NO_3^- anions. Full symbols correspond to Co(II) data, while empty symbols are for Ni(II) [29].

In thermodynamic studies, the ionic strength of the solution is usually controlled by an inert salt at high concentration with respect to the reactants. In previous speciation studies in $[C_4mim][Tf_2N]$ [32,36,63] the IL was assumed to be fully dissociated and that theionic strength (for $[C_4mim][Tf_2N]$ ~ 3.4 mol L^{-1}) was practically unaffected by the complex formation. It should be noted that this assumption is not rigorous, as, on the basis of the analysis of ion diffusion and conductivity data, it was shown that ion pair formation occurs in ILs [64,65]. Specifically, the "Walden plot" (log(molar conductivity, Λ) *vs.* log(reciprocal viscosity η^{-1}),) for $[C_4mim][Tf_2N]$ shows a deviation from a fully dissociated reference electrolyte (KCl aqueous solution) showing that ion pairing is present [65]. However, the ion association in ILs does not seem to give a comprehensive picture, as charge transfer, should also be considered [66,67]. In a recent review [68] it was estimated that for $[C_4mim][Tf_2N]$ the ion dissociation (=[free ions]/[total ions]) is in the 0.60–0.64 range.

As far as the solvated metal ion is considered, it has been previously [63] proposed that the nature of the reacting species (*i.e.* the negatively charged cobalt-containing species in Eq. (2)) is not well defined as in a molecular solvent, due to the strong electrostatic interaction between successive solvation spheres of opposite charge. Based on all the above considerations, and since the activity coefficients of the involved species are not known, the obtained β_j should be considered conditional constants [32].

Stock solutions of $Co(Tf_2N)_2$ and $[C_4mim][NO_3]$ or $[C_4mim][Cl]$ in dry $[C_4mim][Tf_2N]$ were prepared by weighing. The concentration of Co (II) in the stock solution was determined by UV–Vis spectrophotometry [45].

The Co(II) concentration in the samples was kept constant to 0.003 mol L^{-1}, while that of NO_3^- anion was varied from 0 to 0.011 mol L^{-1} corresponding to a total mole of ligand / total moles of metal (R_L) ranging from 0 to 4.35. For Cl^-, the anion concentration ranged from 0 to 0.0067 mol L^{-1} ($0 < R_L < 2.82$).

The absorbance spectra were recorded on a Cary 50 UV–Vis spectrophotometer in a quartz cell of 1 cm path length loaded in the dry box and closed with a Teflon stopper to avoid moisture contamination. The spectra were collected in the 350–850 nm range with a 2 nm spacing. The spectrum of the blank solution was subtracted. Complex formation constants were obtained by multi-wavelength fitting of the absorption spectra using the HypSpec program [69,70]. Between 50 and 100 wavelengths (λ) were selected for the complex formation constant (β_j Eq. (1)) fitting by the analysis of experimental absorbances at different additions of the titrant. The calculated absorbance of one spectrum at a given wavelength was obtained by by the Lamber-Beer law as the sum of the individual absorbances of the different species (j): $A_{\lambda,calc} = l\sum_j \varepsilon_{j,\lambda} C_j$, where l is the optical path length (cm), $\varepsilon_{j,\lambda}$ the molar absorbance (L mol^{-1} cm^{-1}) of the j^{th} species at the wavelength λ and C_j the molar concentration of the j^{th} species. By means of a non-linear regression algorithm, the species concentrations are calculated until the sum of the root-mean-squared difference between the calculated ($A_{\lambda,calc}$) and experimental ($A_{\lambda,exp}$) absorbances at the selected wavelengths is minimized [69,70].

2.3. Isothermal titration calorimetry

Titrations were performed using a TAMIII thermostat (TA Instruments) equipped with a nanocalorimeter and an automated titration apparatus employing a Hamilton syringe (V = 250 μL). The sample and reference cells were loaded under N_2 atmosphere and then transferred in the calorimeter.

In the ITC experiments, the reaction cell contained 0.75 mL of Co(II) solution in $[C_4mim][Tf_2N]$ (C_{Co} = 0.015 mol L^{-1}) stirred by a gold propeller maintained at 50 rpm at 298.15 K. Titrant additions of 10 μL were made with a 15-min delay. The dilution heat was measured by titrating 0.75 mL of pure IL with the $[C_4mim][NO_3]$ or $[C_4mim][Cl]$ solution in the absence of Co(II) and subtracted from the titration data. The $\Delta H_{\beta j}$ values were calculated by means of the HyperDeltaH program [69] by keeping constant the log β_j obtained from the spectrophotometric titrations. In the case of the Co-chloride system the log β_4 was obtained from ITC data, setting the log β_{1-3} at the values obtained by spectrophotometry.

2.4. DFT calculations

Density functional theory calculations were performed for the $[Co(Tf_2N)_iL_j]^{2-i-j}$ complexes. The minimum energy geometries of the high spin Co(II) complexes were obtained by employing the ωB97xD functional [71] and the def2-SVP basis set. Frequency calculations performed for the obtained geometries provided no imaginary vibrational modes, ensuring that these structures corresponded to energy minima. Based on our previous work [29], where X-ray absorption experiments showed that the nitrate anion behaves as a bidentate ligand with Ni(II) in dry $[C_4mim][Tf_2N]$, therefore only this coordination mode was considered in our calculations. All geometry optimizations were performed in Gaussian16 [72].

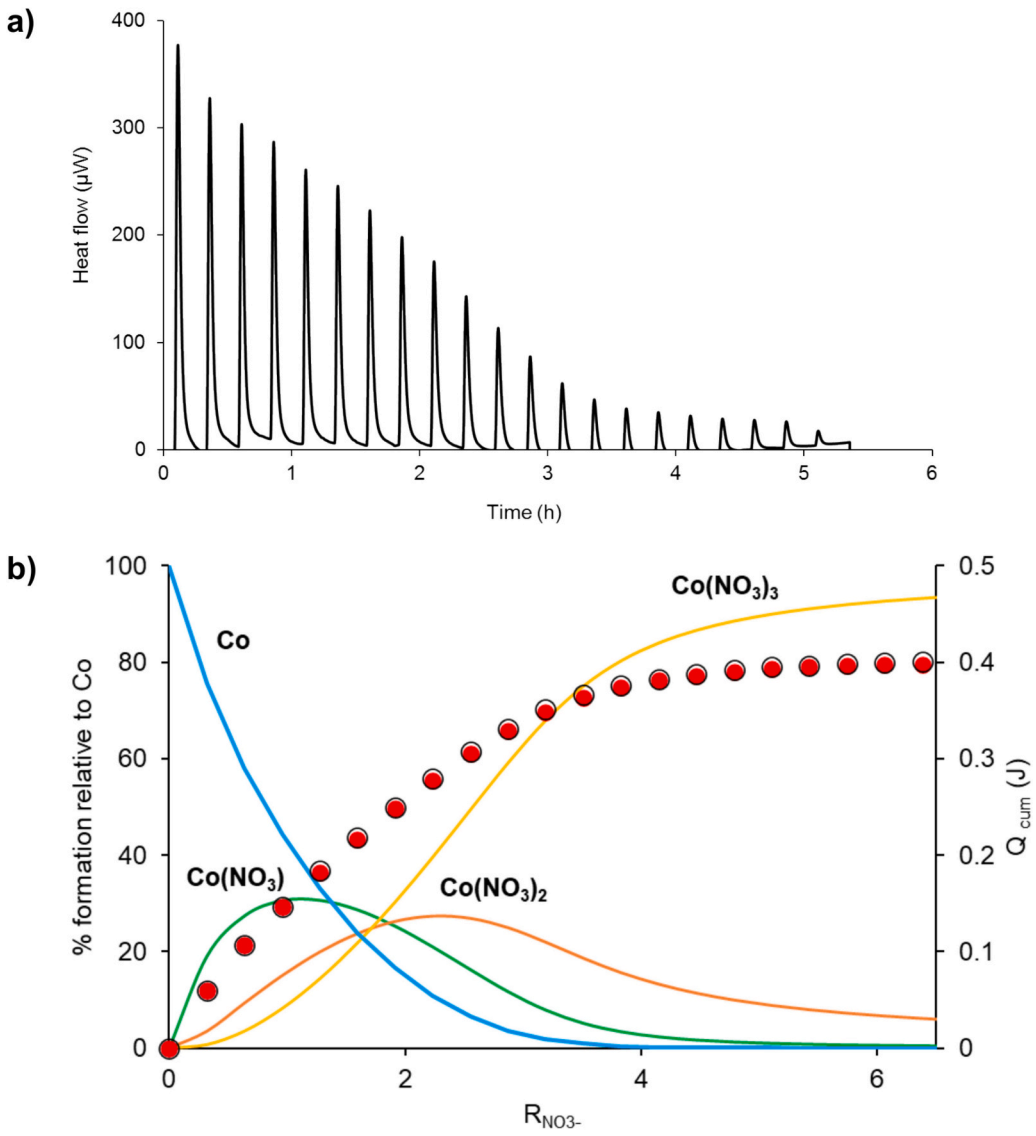

Fig. 3. (a) Calorimetric titration of Co(II) with NO_3^- in dry [C_4mim] [Tf_2N] at 298 K. Initial solution: $V_0 = 0.75$ mL and $C_{Co} = 15$ mM. Titrant solution: $C_L = 362$ mM. Final $R_L = 6.7$. (b) Cumulative heat (Q_{cum}) observed (red circles) and calculated (empty circles) *vs.* the Co/ NO_3^- molar ratio (R_L). The calculated speciation (charges omitted) as a function of the NO_3^- added is also reported. (For interpretation of the references to colour in this figure legend, the reader is referred to the web version of this article.)

2.5. Molecular dynamics simulations

Classical molecular dynamics simulations have been performed employing the non-polarizable force field by Canongia Lopes and Padua [73–75] for the [C_4mim][Tf_2N] IL and the Cl^- and NO_3^- anions. The Lennard-Jones (LJ) parameters of the metal were taken from ref. [76] (the "IOD" set) which provided good agreement with the experimental X-ray absorption data for the solvated Co(II) ion in [C_4mim][Tf_2N] [45]. In our simulations, the $Co(NO_3)_j$ and $CoCl_j$ (j = 1–4) units were considered as solutes as previously done for the Ni(II) ion [29]. For the complexes with the nitrate anion, the bidentate coordination mode was assumed on the basis of the minimum energy structures and obtained by DFT calculations and previous theoretical and experimental results for the similar Ni(II) cation [29]. The intramolecular interactions were modeled using harmonic bonds and angles, where the equilibrium distances and force constants were obtained from DFT calculations (Table S1). Nitrate anions were kept planar and N—O distances were constrained. The point charges for the $Co(NO_3)_j$ and $CoCl_j$ were calculated to fit to the electrostatic potential according to the Merz-Kollman scheme [77] in the presence of a continuum solvent introduced by a SMD polarizable model [78] (Table S2) with the parameters given for the [C_4mim][Tf_2N] [79]. The composition of the simulated boxes for the two sets of calculations is reported in Table S3.

Non-bonded van der Waals (vdW) interactions were represented by LJ potential, for which cross terms were constructed with the Lorentz-Berthelot combining rules. A cut-off radius of 15 Å was employed for all the non-bonded interactions. Simulated systems were first equilibrated in NVT conditions for 20 ns at 500 K and then cooled down to 300 K. Production MD was run for 50 ns in NVT conditions at 300 K. In all calculations, a 2 fs time step has been employed, and the temperature was kept constant by the velocity rescaling algorithm. All MD simulations were run in GROMACS 2020.5 [80].

3. Results and discussion

When a negatively charged ligand (X^-) binds the Co(II) ion in [C_4mim][Tf_2N] solution, the weakly coordinating [Tf_2N]$^-$ anions are displaced as described by the equilibrium reaction (2):

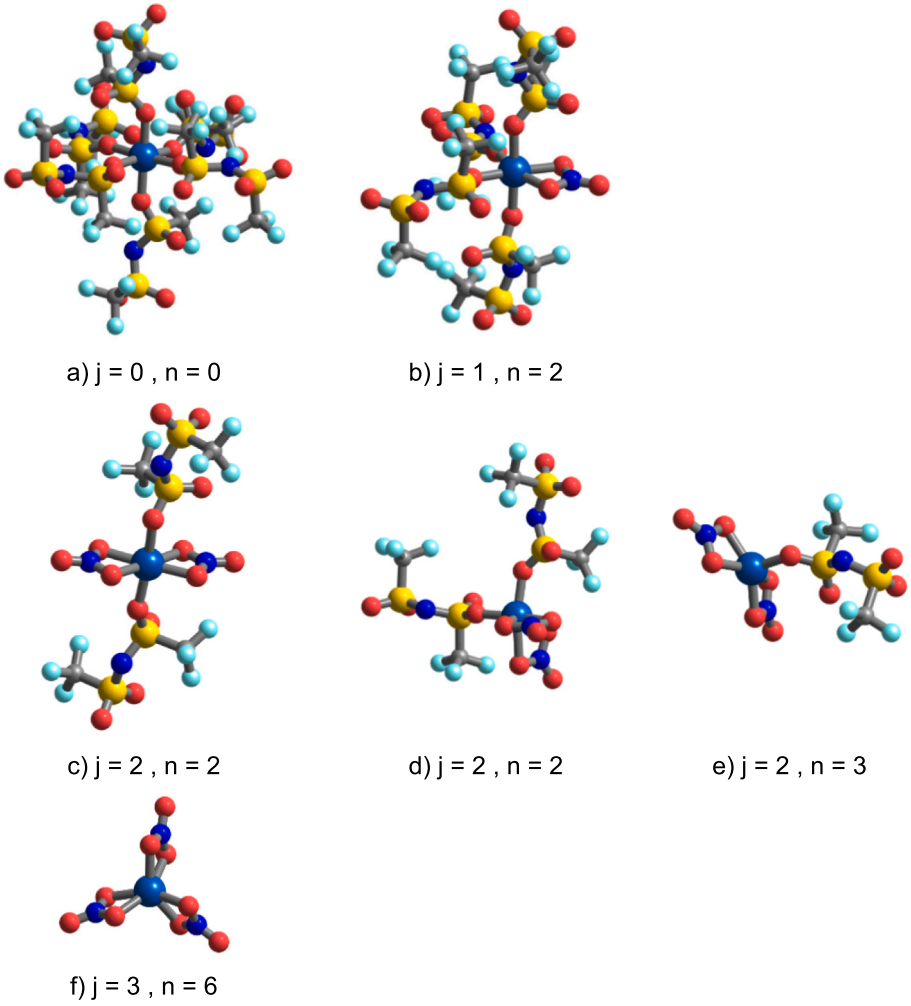

Fig. 4. Minimum energy structures of the $[Co(Tf_2N)_{6-n}(NO_3)_j]^{(4-j+n)-}$ complexes ($0 \leq j \leq 3$).

$$\left[Co(Tf_2N)_6\right]^{4-} + jX^- \leftrightarrows \left[Co(Tf_2N)_{6-n}(X)_j\right]^{n-j-4} + n[Tf_2N]^- \quad (2)$$

In dry $[C_4mim][Tf_2N]$ [45], the nature of the Co(II) reactant ($[Co(Tf_2N)_6]^{4-}$) in Eq. (2) has been previously defined by means of EXAFS experiments and MD simulations which evidenced the coordination of 6 monodentate $[Tf_2N]^-$ anions. The same solvation structure was also obtained for other bivalent metals, Zn(II) and Ni(II) [43–45]. The experimental thermodynamic parameters of complex formation are determined by the enthalpic contributions related to the bond breaking/formation and solvation/desolvation of all species involved as well as entropic terms reflecting the changes of the degrees of freedom in the system.

3.1. Nitrate complexes

Spectrophotometric titrations were performed by recording the UV–Vis absorption spectra in the 400–800 nm wavelength range (Fig. 1) where Co(II) compounds exhibit characteristic *d–d* transition bands sensitive to the metal coordination environment and ligand field strength [45].

The spectrum of the Co(II) solution in the absence of nitrate anion (red line in Fig. 1) presents a maximum at $\lambda = 548$ nm (similar that previously observed in $[C_4mim][Tf_2N]$ [45]) and an increase of intensity occurs upon addition of titrant (Fig. 1). The spectral changes in the absorption bands of $Co(Tf_2N)_2$ in $[C_4mim][Tf_2N]$ upon addition of nitrate solution indicate that the starting octahedral coordination is maintained by the metal ion (Fig. 1) [27,45].

The best fit of the absorbance data is compatible with a model including three successive 1:1, 1:2, and 1:3 species. In the solid state, structures containing the $[Co(NO_3)_4]^{2-}$ anion with three coordinated bidentate nitrates and the fourth monodentate were obtained [81]. However, the introduction of an additional 1:4 species in the analysis of the spectrophotometric data, even if considered as non-absorbing, was rejected by the fitting software. Experimental molar absorbances (Fig. S1) clearly indicate that an octahedral coordination mode of the formed species is maintained by the metal ion along the titration. The complex formation constants of the Co(II) complexes with NO_3^- are reported in Table 1 together with related enthalpy and entropy values. A similar result was obtained for the speciation of Ni(II) with NO_3^- in $[C_4mim][Tf_2N]$ where up to three successive $Ni(NO_3)_j$ species of decreasing relative stability were found (Fig. 2) [29].

Contrary to what is observed in water, NO_3^- is a strong ligand for this Co(II) ion in this IL. This is expected based on the poor solvating strength of the $[Tf_2N]^-$ anion with respect to water, which is reflected by the positive single ion free energy of transfer from water to $[C_4mim][Tf_2N]$ (ΔG_{trans}(water → $[C_4mim][Tf_2N]$) = 6.6 kcal mol^{-1}) previously calculated for Co(II) [45]. This result is in agreement with the positive ΔG_{trans}(water → $[C_4mim][Tf_2N]$) values for other bivalent ions such as Zn(II) or Cu(II) calculated on the basis of experimental data [44,82]. Interestingly the stability of the 1:1 complex formed by Zn(II) with the neutral chelating ligand ethylenediammine in $[C_2mim][Tf_2N]$ is lower than in water [31], while the 1:2 is higher indicating that the ligand and the formed metal species solvation are also important factors in

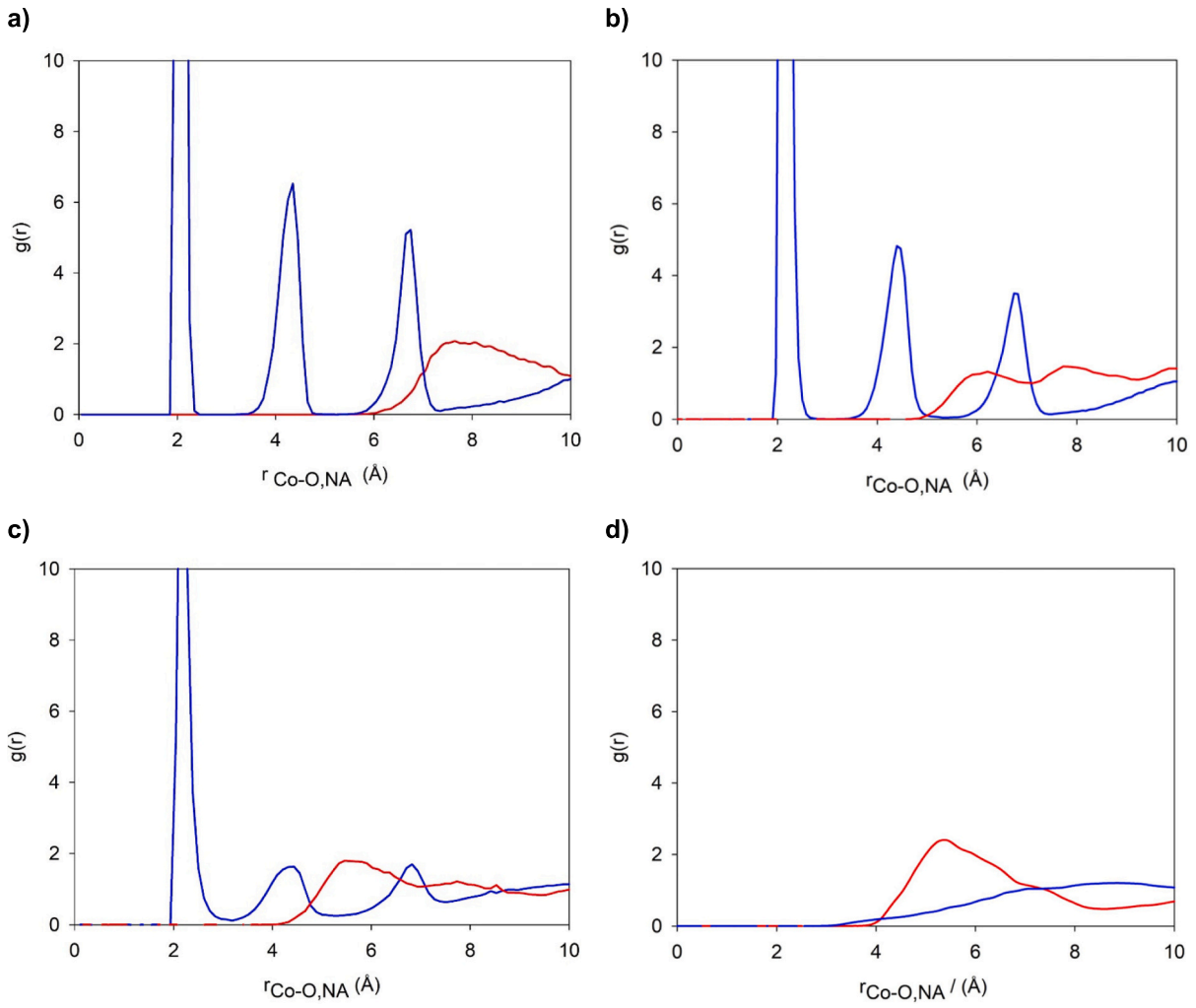

Fig. 5. Co—O $[Tf_2N]^-$ (blue) and Co—NA $[C_4mim]^+$ (red) for the simulated $[Co(Tf_2N)_{6-n}(NO_3)_j]^{n-j-4}$ complexes: (a) j = 0; (b) j = 1; (c) j = 2; (d) j = 3. (For interpretation of the references to colour in this figure legend, the reader is referred to the web version of this article.)

Table 2
Position (Å) and integration number of the first maximum of the Co-O$[Tf_2N]^-$ and Co-NA $[C_4mim]^+$ radial distribution functions (Fig. 5 and Fig. 10).

Solute	j	r_{max} Co-O $[Tf_2N]^-$ (Å)	n_O	r_{max} Co-NA $[C_4mim]^+$ (Å)	n_{NA}[a]
	0	2.05	6.0	7.65	–
[Co	1	2.14	4.5	6.24	–
$(Tf_2N)_n(NO_3)_j]^{2-}_{n-j}$	2	2.16	2.3	5.50	–
	3	8.52[b]	–	5.31	11.6 (5.8)
	1	2.15	5.0	7.85	–
	2	2.25	2.7	5.36	–
$[Co(Tf_2N)_n(Cl)_j]^{2-n-}_{j}$	3	2.25	1.0	5.48	15.6 (7.8)
	4	8.85	–	4.83	14.8 (7.4)

[a] n_{NA} not reported for broad distributions without well-defined peaks. In parentheses, the estimated number of cations.
[b] $[Tf_2N]^-$ is not coordinated.

determining the relative stabilities in different media.

As far as non-aqueous solvents are considered, the only available data are relative to the formation of the 1:1 species in acetonitrile (log K_1 = 5.45 [83] and 4.02 [84]). It should be noted that no other species were obtained by data refinement in Refs. [83, 84].

The profile of the calorimetric titration in Fig. 3a shows that the overall process is exothermic, as previously observed for the formation of nitrate complexes with Ni(II) in $[C_4mim][Tf_2N]$. The analysis of ITC data (Fig. 3b) provided an excellent agreement between calculated and observed heat data and confirmed the speciation obtained by UV–Vis titrations. As previously noted for complex formation between trivalent metal ions and nitrate in $[C_4mim][Tf_2N]$ the $\Delta H_{\beta j}$ are all negative and $\Delta S_{\beta j}$ positive [36]. On the contrary, in the water-saturated IL, the complex formation was only entropy-driven [36] as usually found in aqueous solutions when charge neutralization occurs upon complex formation [85]. It is interesting to note that the 1:2 species presents a much less negative ΔH_{Kj} with respect to the 1:1 species with an entropic term which remains close ($T\Delta S_{K1}$ and $T\Delta S_{K2}$ are 13.4 and 10.4 kJ mol^{-1} respectively). Moreover, the 1:3 complex has an enthalpy nearly equal to that of the 1:1, but with a much less favorable entropic term ($T\Delta S_{K3}$ = −1.2 kJ mol^{-1}). This trend of the stepwise thermodynamic parameters could be due to a variable desolvation pattern upon nitrate coordination, as well as significant changes in the outer-sphere ionic structure.

To have a structural model of the species in solution, it should be recalled that in a previous work on Ni(II)/nitrate complexation in $[C_4mim][Tf_2N]$ it was shown that NO_3^- anion acted as a bidentate ligand on the basis of computational methods (MD simulations) and X-ray absorption spectroscopy [29]. While this binding mode can be assumed also for Co(II), the number of anions released from the metal first coordination sphere ($n[Tf_2N]^-$ in eq. 1) can be variable depending on the complexation step.

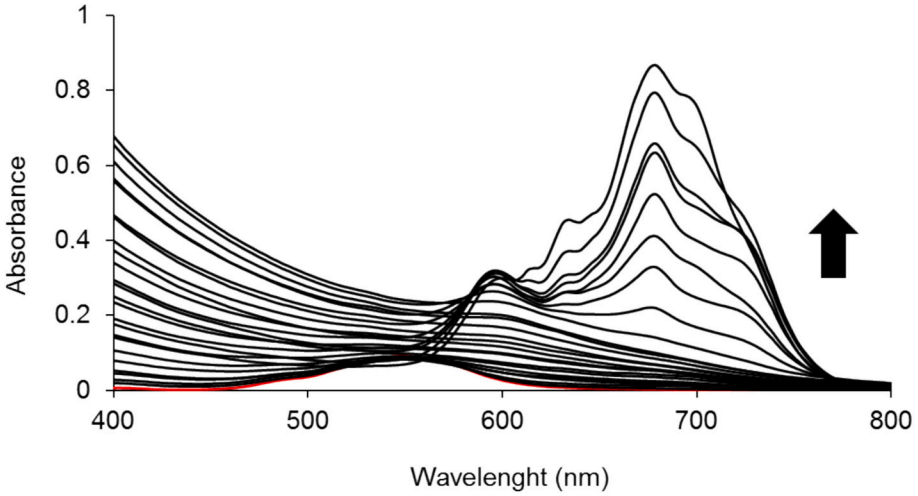

Fig. 6. Spectrophotometric titration of Co(II) with Cl^- in dry $[C_4mim][Tf_2N]$ at 298 K. Initial solution: $V_0 = 1.82$ mL and $C_{Co} = 3$ mM (red spectrum). Titrant solution: $C_L = 33$ mM. Final ratio Co(II): $Cl^- = 2.82$. The black arrow shows the direction of spectra evolution. (For interpretation of the references to colour in this figure legend, the reader is referred to the web version of this article.)

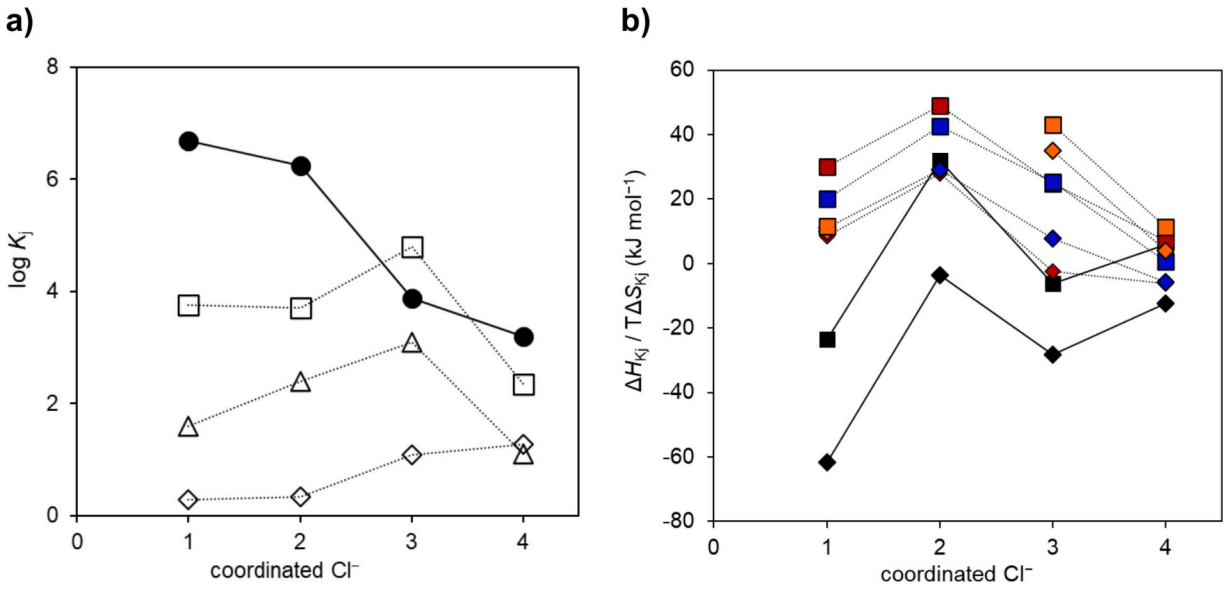

Fig. 7. Stepwise stability constant for the $CoCl_j$ species in log K_j plotted against the number of coordinated chlorides: ● $[C_4mim][Tf_2N]$, □ DMF, △ DMSO, ◊ NMF; (b) ΔH_{Kj} (diamonds) and $T\Delta S_{Kj}$ (squares) for $[C_4mim][Tf_2N]$ (black), DMF (red), DMSO (blue), NMF (orange). Data from Refs. [87–89]. (For interpretation of the references to colour in this figure legend, the reader is referred to the web version of this article.)

To obtain further insights into the possible cobalt-containing species in solution, DFT calculations were performed. The minimum energy structures of the $[Co(Tf_2N)_{6-2j}(NO_3)_j]^{-4+j}$ complexes ($0 \leq j \leq 3$) are shown in Fig. 4 and the obtained Co-X bond lengths are reported in Table S4. Only one type of 1:1 and 1:3 species has been considered ($[Co(Tf_2N)_4(NO_3)]^{3-}$ and $[Co(NO_3)_3]^-$, b and f in Fig. 4) while for the 1:2 several possibilities, including 6 and 5-coordination, were taken into account. As for the $[Co(Tf_2N)_2(NO_3)_2]^{2-}$ species (c and d in Fig. 4), a mixture of the c and d isomers is likely to be present in solution as the calculated difference in energy is only of ~1.0 kcal mol^{-1}.

Thermodynamic results could be therefore interpreted by assuming the release of 2 $[Tf_2N]^-$ anions in the formation of the 1:1 species, followed by the replacement of 2 or 3 $[Tf_2N]^-$ anions by nitrate in the 1:2 species, which would explain the less favorable stepwise enthalpy term with respect to 1:3 and 1:1. The negative and small $T\Delta S_{K3}$ is compatible with the coordination of a third nitrate and the release of either 1 or 2 $[Tf_2N]^-$ anions.

In order to obtain a dynamic picture of the species in solution and the surrounding ionic environment, MD simulations were also carried out. In these simulations NO_3^- anions were constrained to be coordinated to the Co(II) ion while $[Tf_2N]^-$ could be exchanged with the bulk liquid phase.

The radial distribution functions, g(r), for the centers Co—O and Co—NA (where O is the oxygen of the —SO_2— group of the anion and NA are the aromatic nitrogen atoms of $[C_4mim]^+$) are shown in Fig. 5. The obtained g(r) for the starting Co(II) solvate in agreement with previous experimental and simulation findings [43,45] and evidence the presence of coordinated O at 2.05 Å and two further maxima corresponding to the "free" oxygen atoms of the coordinated anion. Also in this study, bidentate $[Tf_2N]^-$ anions are not observed, even in the complexes with nitrate. The position of the first $g(r_{Co\text{-}O})$ maxima are in good agreement with the previous work [45] and are slightly shifted towards higher values when the 1:1 and 1:2 species are considered. When one bidentate nitrate is introduced in the coordination sphere of

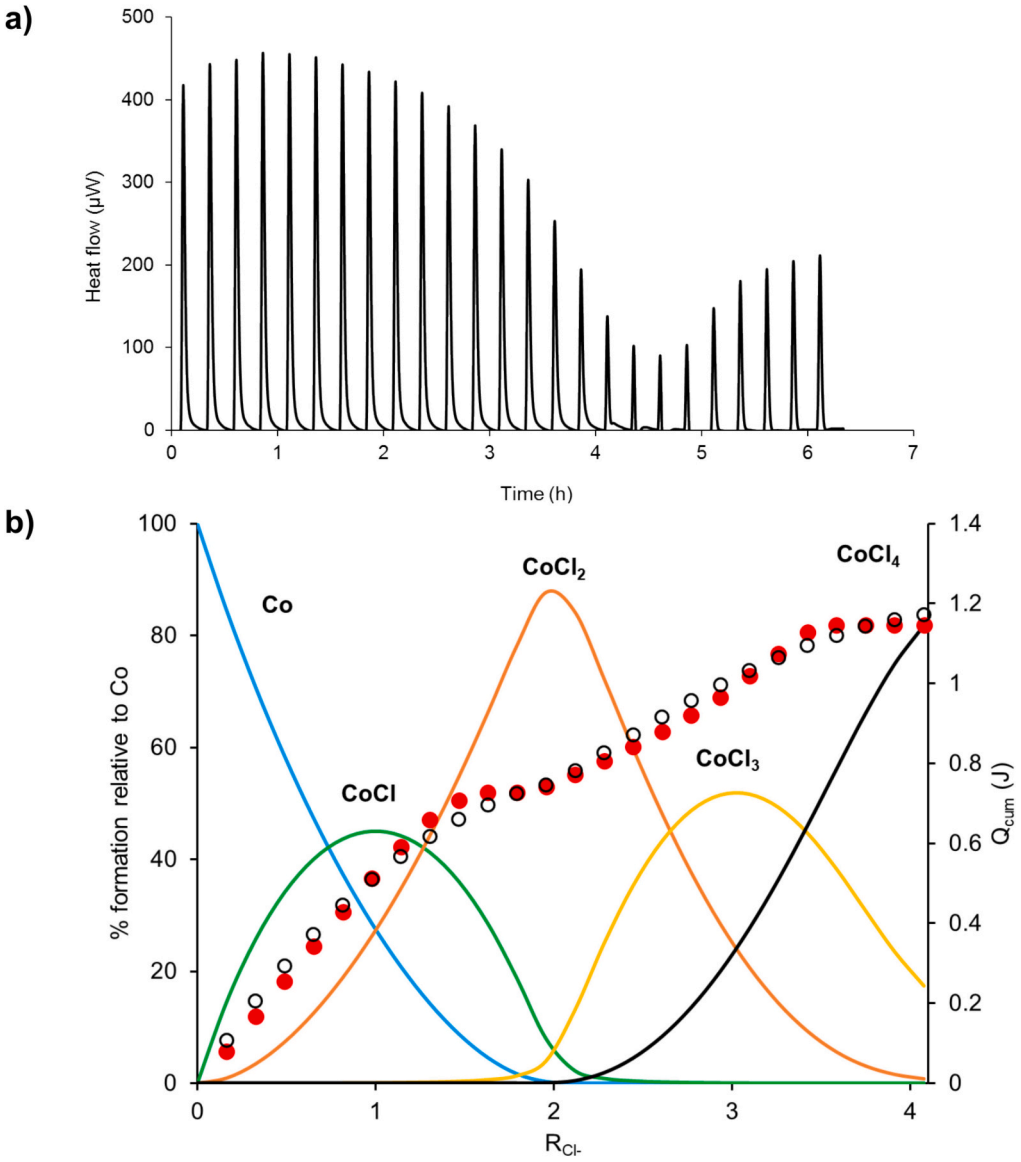

Fig. 8. (a) Calorimetric titration of Co(II) with Cl^- in dry [C_4mim][Tf_2N] at 298 K. Initial solution: $V_0 = 0.75$ mL and $C_{Co} = 15$ mM. Titrant solution: $C_L = 186$ mM. Final ratio Co(II): $Cl^- = 0$–4.09. (b) Cumulative heat (Qcum) observed (red circles) and calculated (empty circles) on the basis of the log β_j and $\Delta H_{\beta j}$ values reported in Table 1 *vs* the Co(II)/Cl^- molar ratio (R_{Cl-}). The corresponding Co(Cl)$_j$ speciation (charges omitted) as a function of the Cl^- added is reported.

Table 3
Overall (log β_j) and stepwise (log K_j) stability constants and thermodynamic parameters (kJ mol^{-1}) relative to the reaction: Co(II) + jCl^- ⇆ [Co(Cl)$_j$]$^{2-j}$ in [C_4mim][Tf_2N] ($T = 298.15$ K). Standard deviations are reported in parentheses.

j	log β_j	$\Delta G_{\beta j}$	$\Delta H_{\beta j}$	$T\Delta S_{\beta j}$	log K_j	ΔG_{Kj}	ΔH_{Kj}	$T\Delta S_{Kj}$
1	6.68(4)	−38.1	−61.6(1)	−23.5	6.68	−38.1	−61.6	−23.5
2	12.92(6)	−73.7	−65.3(9)	8.5	6.24	−35.6	−3.7	31.9
3	16.79(3)	−95.8	−93.5(6)	2.3	3.87	−22.1	−28.3	−6.2
4	20(1)	−114.1	−105.9(7)	8.2	3.2	−18.3	−12.4	5.9

the metal ion (*i.e.* to obtain the 1:1 species), the number of coordinated [Tf_2N]$^-$ anions decreases from 6 to ~4.5 (Table 2). When a second nitrate is coordinated to Co(II), the number of coordinated [Tf_2N]$^-$ anions is further reduced to ~2.3. Within the simulation time, the formation of the [Co(Tf_2N)(NO_3)$_2$]$^-$ complex was not observed. Finally, in the 1:3 species, no [Tf_2N]$^-$ anion remains coordinated to the metal ion. This result supports the hypothesis that two nitrate anions are released at the first complexation step and that the 1:3 species has no coordinated [Tf_2N]$^-$ anions.

The g($r_{Co\text{-}NA}$), which provides information on the distribution of first shell of cations around the anionic metal-containing species, reveals a contraction of the volume in the complexes with the nitrate (Fig. 5), which is expected as this ligand is smaller than the [Tf_2N]$^-$ anion. The strongly negative entropy of solvation calculated previously for Co(II) and other bivalent metals [43–45] was explained by a strong ordering of the IL imposed by the metal ion, which is broken when the complexes are formed. This observed change in the structure of the IL surrounding the metal-containing species, and the reduction of the volume occupied

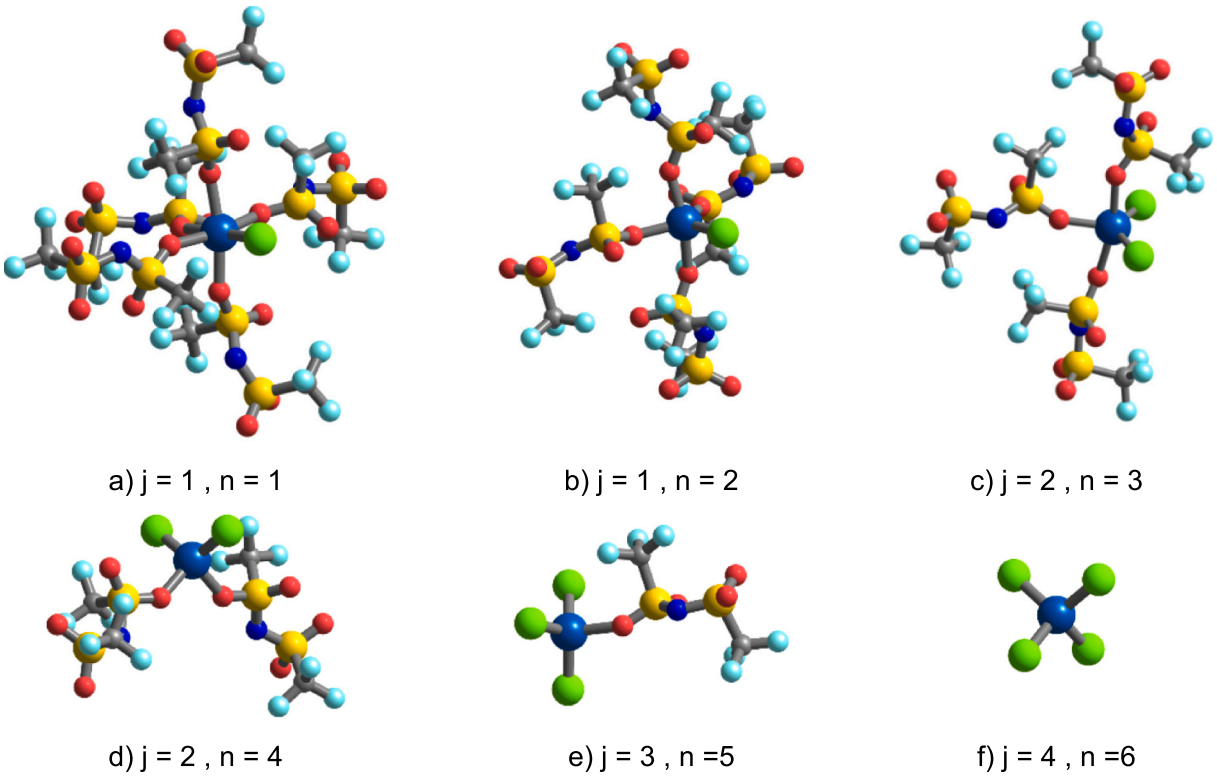

Fig. 9. Minimum energy structures of the $[Co(Tf_2N)_{6-n}Cl_j]^{-4+j+n}$ complexes ($1 \leq j \leq 4$),

by the latter, should have a relevant importance in determining the entropy changes upon complex formation.

3.2. Chloride complexes

The UV–Vis spectra of $Co(Tf_2N)_2$ in dry $[C_4mim][Tf_2N]$ at increasing Cl^- content are shown in Fig. 6. The best fit of absorbance data was obtained with a model including three $CoCl_j$ species (j = 1–3) which present higher stabilities than the corresponding ones formed with nitrate (Table 1 and Fig. 7). These much higher stabilities of the complexes formed by Co(II) with Cl^- ion with respect to those with NO_3^- is also in agreement with the observation that this anion is able to displace nitrate from the metal coordination sphere even in the nitrate-containing IL ($[HO(CH_2)_2mim]NO_3$) [86].

The absorbance trend in the 500–750 nm range observed in the spectra at Cl/Co ratios ≥2.0 (Fig. S2) is indicative of the formation of tetrahedral species, thus, as previously found for complex formation in non–aqueous coordinating solvents [87,88], a change of coordination geometry of the metal ion occurs when the 1:2 species is formed.

Calorimetric data shown in Fig. 8 presents a completely different trend with respect to the titration with nitrate. The fit of ITC data (Fig. 8b) allowed the estimation of the log βj relative to the 1:4 species (Table 3). When the latter species was inserted in the model employed for the UV–Vis titration, some improvement of the goodness of fit was observed (*i.e.* a lower residual sum of squares), however any further refinement was unsuccessful. This was probably due to the small number of points at Cl:Co ratios sufficiently high to allow the formation of a significant amount of $CoCl_4$.

The overall enthalpies of complex formation in dry $[C_4mim][Tf_2N]$ are all negative, while the formation entropy is negative for the 1:1 species only.

The calculated stability constants in dry $[C_4mim][Tf_2N]$ are several orders of magnitude higher than those determined in aqueous solutions and other molecular solvents [87–90] as expected on the basis of the weak coordinating strength of the $[Tf_2N]^-$ anion. This is evident when our results are compared with those reported in the non-aqueous solvents dimethylsulfoxide (DMSO), *N*,*N*-dimethylformamide (DMF) and *N*-methylformamide (NMF) [87–89] (Table S5 and Fig. 7) where complex formation is solely entropy-driven with large positive $\Delta H_{\beta j}$ values. As evidenced in Fig. 7a, the stepwise stability constants decrease monotonically in the IL, differently from those in the molecular solvents.

Stepwise enthalpies, with the exception of the formation of the 1:2 are significantly more negative than nitrate, indicating a stronger interaction of the Cl^- anion with the metal center (Table 1). Also, ΔS_{Kj} differs markedly from the previous ligand and can be interpreted by a different desolvation of the Co-containing species at each step.

The positive stepwise entropic term for the formation of the 1:2 species ($T\Delta S_{K2} = 32.0$ kJ mol^{-1}) coupled to the relatively low enthalpy ($\Delta H_{K2} = -3.7$ kJ mol^{-1}) can be interpreted by the strong desolvation of the metal ion, which leads to the release of several solvent molecules upon coordination of one ligand [23,25]. Therefore, it can be proposed that the change of coordination mode of cobalt occurs when the second chloride is added, as also found previously in molecular solvents [88–90]. This is clearly different from the result obtained for the 1:2 Co:NO_3^- which presents a less positive $T\Delta S_{K2}$ and more negative ΔH_{K2} evidencing that desolvation of the metal is notably different in the two systems.

The DFT optimized structures of two possible 1:1 Co:Cl^- species are shown in Fig. 9. For the 1:1 species, both the octahedral $[Co(Tf_2N)_5Cl]^{4-}$ and the trigonal bipyramidal $[Co(Tf_2N)_4Cl]^{3-}$ structures were obtained. However, MD simulations evidence the presence of only 5 coordinated $[Tf_2N]^-$ anions as in the complex shown in Fig. 9. It should be noted that the octahedral coordination of the metal ion in the 1:1 Co:Cl species was also previously assumed in concentrated chloride solutions [91].

Several 1:2 Co:Cl species were considered ($[Co(Tf_2N)_4Cl_2]^{4-}$, $[Co(Tf_2N)_3Cl_2]^{3-}$, $[Co(Tf_2N)_2Cl_2]^{2-}$) for the DFT calculations. However, the geometry optimization of the starting octahedral complexes ($[Co(Tf_2N)_4Cl_2]^{4-}$) led to the spontaneous dissociation of one $[Tf_2N]^-$ to give a tetrahedral $[Co(Tf_2N)_2Cl_2]^{2-}$ or penta-coordinated $[Co(Tf_2N)_3Cl_2]^{3-}$ species (Fig. 9). Thus, DFT calculations suggest that the Co-containing

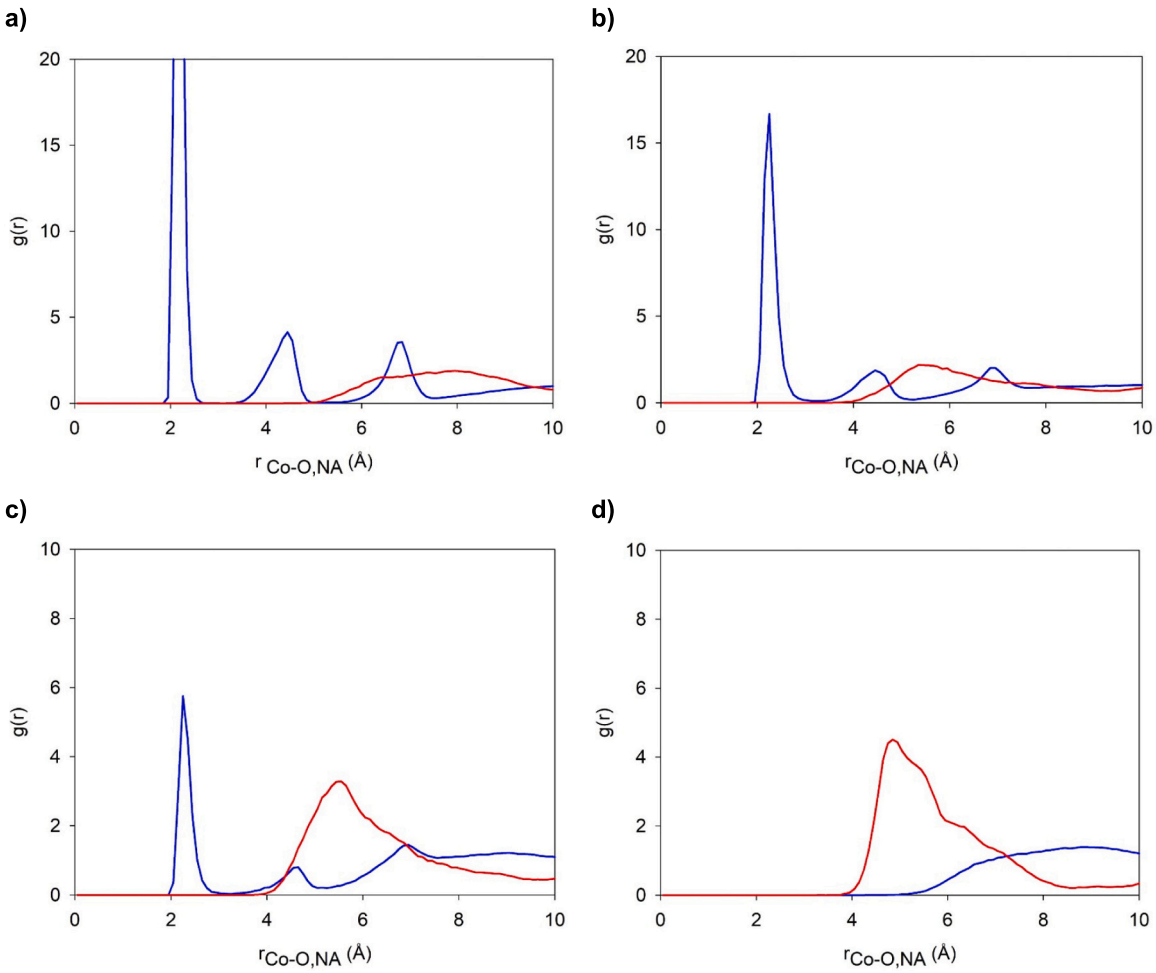

Fig. 10. Co—O $[Tf_2N]^-$ (blue) and Co-NA $[C_4mim]^+$ (red) for the simulated $[Co(Tf_2N)_{6-n}Cl_j]^{n-j-4}$ complexes: (a) j = 1; (b) j = 2; (c) j = 3; (d) j = 4. (For interpretation of the references to colour in this figure legend, the reader is referred to the web version of this article.)

species in solution could have either 2 or 3 coordinated $[Tf_2N]^-$ anions.

The analysis of the g(r) for the 1:2 Co:Cl species (Table 2) shows that the number of coordinated oxygen atoms is ~2.7, supporting the presence of a mixture of 4- and 5-coordinated $CoCl_2$ species in solution. Therefore, computational results support the occurrence of a large desolvation upon going from the 1:1 to 1:2 species, due to the release of 2 or 3 $[Tf_2N]^-$ anions in a single step. This is also in agreement with the largely positive stepwise entropy ($T\Delta S_{K2}$) and also the fact that ΔH_{K2} is much less negative than ΔH_{K1}. Interestingly, the g(r) for the Co-NA centers displays a net decrease of the maximum position (from 7.85 to 5.36 Å, Table 2) indicating that a significant reordering of the ions surrounding the anionic metal species occurs in this complexation step. This net decrease of the occupied volume and charge of the metal complex (from −4 in the 1:1 to −2 in the tetrahedral $CoCl_2$ species) could also be responsible for the highly positive ΔS_{K2}. As for the 1:3 species, the UV–Vis spectra clearly indicate a tetrahedral species, which is also supported by DFT and MD results, which, coherently, point towards a tetrahedral complex with only one $[Tf_2N]^-$ coordinated (Table 2 and Fig. 9). This agrees with the value of ΔH_{K3} which is much more negative than ΔH_{K2} and can be related to the release of 1 or 2 $[Tf_2N]^-$ anions. Also, the maximum position of the g(r) for Co-NA does not display a marked shift as in the previous system, rather, the intensity increases suggesting a more rigid cationic structure around the anionic complex. Finally, MD simulations confirm that the tetrahedral $[CoCl_4]^{2-}$ has no anions coordinated. This result is in agreement with EXAFS data in chloride-containing ILs which show that cobalt is coordinated by four chlorides only [92]. The small and positive $T\Delta S_{K4}$ and the relatively small ΔH_{K4} are compatible with the replacement of the remaining $[Tf_2N]^-$ by a chloride anion.

4. Conclusions

In this study, we investigated the complex formation of Co(II) ions with nitrate and chloride anions in the dry IL $[C_4mim][Tf_2N]$. Through a combination of UV–Vis spectrophotometry and ITC, we established that both anions effectively coordinate with Co(II) leading to stable complex formation in this IL. The findings revealed distinct speciation and thermodynamic parameters associated with the complex formation, which can be interpreted by considering the balance of the energetics related to the bond breaking/forming and the solvent reorganization. Absorption spectra, along with DFT calculations and MD simulations allowed us to provide structural information on the species in solution. The entirety of the information obtained shows that the octahedral coordination is maintained with increasing nitrate:Co ratio in solution. Nitrate anions replace 2 $[Tf_2N]^-$ per complexation step, and it is shown that two equally stable octahedral 1:2 species can be present. In the final 1:3 complex all $[Tf_2N]^-$ anions have been released. The main finding regarding complex formation with chloride is the presence of a net switch of coordination number on going from the octahedral 1:1 species, to 1:2 species, which is proposed to be a mixture of a tetrahedral and penta-coordinated metal ions. The higher 1:3 and 1:4 species are exclusively tetrahedral, as evidenced by absorption spectra and theoretical models. In both cases it has been evidenced that the IL structure around the solute undergoes notable changes due to the decrease in

volume and charge of the cobalt-containing species.

The thermodynamic and structural insights obtained in this work can support the design of more efficient processes of cobalt separations and recovery by electrodeposition.

CRediT authorship contribution statement

Martina Sanadar: Writing – review & editing, Writing – original draft, Methodology, Investigation, Formal analysis, Data curation, Conceptualization. **Anđela Kovačević:** Methodology, Investigation, Formal analysis, Data curation. **José Alejandro Ricardo García:** Methodology, Investigation, Formal analysis, Data curation. **Marilena Tolazzi:** Writing – review & editing, Investigation, Funding acquisition, Data curation. **Andrea Melchior:** Writing – review & editing, Writing – original draft, Supervision, Resources, Investigation, Formal analysis, Data curation.

Declaration of competing interest

The authors declare that they have no known competing financial interests or personal relationships that could have appeared to influence the work reported in this paper.

Acknowledgments

This work was carried out within the scope of the FREECOVER project (grant agreement #101182579) under the European Community's Horizon Europe Program HORIZON-MSCA-2023-SE-01. This research was also supported by the University of Udine, in the framework of the Strategic Plan 2022-25 – Interdepartmental Research Project ESPeRT. AM&AK acknowledge the National Operational Program 2014-2020 "Ph.D. Programmes on Green Topics". MT acknowledges the Italian Ministry for University and Research for funding through the PRIN2022 call with the project "Wastezilla" (2022HYH95P).

Declaration of competing interest

The authors declare the following financial interests/personal relationships which may be considered as potential competing interests: Andrrea Melchior reports financial support was provided by European Commission. If there are other authors, they declare that they have no known competing financial interests or personal relationships that could have appeared to influence the work reported in this paper.

Appendix A. Supplementary data

Supplementary data to this article can be found online at https://doi.org/10.1016/j.molliq.2025.128162.

Data availability

Data will be made available on request.

References

[1] M.R. Asrami, N.N. Tran, K.D.P. Nigam, V. Hessel, Solvent extraction of metals: role of ionic liquids and microfluidics, Sep. Purif. Technol. 262 (2021) 118289, https://doi.org/10.1016/j.seppur.2020.118289.
[2] P.A. Yudaev, E.M. Chistyakov, Ionic liquids as components of Systems for Metal Extraction, ChemEngineering 6 (2022) 6, https://doi.org/10.3390/chemengineering6010006.
[3] M. Regel-Rosocka, M. Wisniewski, Ionic liquids in separation of metal ions from aqueous solutions, in: S. Handy (Ed.), Appl Ion Liq Sci Technol, InTech, 2011, pp. 375–398, https://doi.org/10.1016/B978-0-444-63257-9.00004-3.
[4] A. Kovačević, M. Tolazzi, M. Sanadar, A. Melchior, Hydrometallurgical recovery of metals from spent lithium-ion batteries with ionic liquids and deep eutectic solvents, J. Environ. Chem. Eng. 12 (2024) 113248, https://doi.org/10.1016/j.jece.2024.113248.
[5] A. Kovacevic, J.A. Ricardo García, M. Tolazzi, A. Melchior, M. Sanadar, Selective co(II) and Ni(II) separation using the Trihexyl(tetradecyl)phosphonium Decanoate ionic liquid, Molecules 29 (2024), https://doi.org/10.3390/molecules29194545.
[6] P. Meshram, N. Agarwal, Abhilash, A review on assessment of ionic liquids in extraction of lithium, nickel, and cobalt vis-à-vis conventional methods, RSC Adv. 15 (2025) 8321–8334, https://doi.org/10.1039/D4RA08429B.
[7] P.K. Mohapatra, Actinide ion extraction using room temperature ionic liquids: opportunities and challenges for nuclear fuel cycle applications, Dalton Trans. 46 (2017) 1730–1747, https://doi.org/10.1039/c6dt04898f.
[8] K. Binnemans, Lanthanides and actinides in ionic liquids, Chem. Rev. 107 (2007) 2592–2614, https://doi.org/10.1016/B978-0-08-097774-4.00228-X.
[9] Q. Zhang, Q. Wang, S. Zhang, X. Lu, X. Zhang, Electrodeposition in ionic liquids, ChemPhysChem 17 (2016) 335–351, https://doi.org/10.1002/cphc.201500713.
[10] F. Liu, Y. Deng, X. Han, W. Hu, C. Zhong, Electrodeposition of metals and alloys from ionic liquids, J. Alloys Compd. 654 (2016) 163–170, https://doi.org/10.1016/j.jallcom.2015.09.137.
[11] K. Motobayashi, Y. Shibamura, K. Ikeda, Origin of a high Overpotential of co electrodeposition in a room-temperature ionic liquid, J. Phys. Chem. Lett. 11 (2020) 8697–8702, https://doi.org/10.1021/acs.jpclett.0c02605.
[12] K. Motobayashi, H. Nakagawa, Y. Shibamura, K. Ikeda, Origin of temperature-dependent Overpotential of co electrodeposition in an ionic liquid, J. Phys. Chem. C 128 (2024) 819–826, https://doi.org/10.1021/acs.jpcc.3c07750.
[13] F. Ilyas, M. Ishaq, M. Jabeen, M. Saeed, A. Ihsan, M. Ahmed, Recent trends in the benign-by-design electrolytes for zinc batteries, J. Mol. Liq. 343 (2021) 117606, https://doi.org/10.1016/j.molliq.2021.117606.
[14] Y. Liu, Y. Elias, J. Meng, D. Aurbach, R. Zou, D. Xia, Q. Pang, Electrolyte solutions design for lithium-sulfur batteries, Joule 5 (2021) 2323–2364, https://doi.org/10.1016/j.joule.2021.06.009.
[15] J. Piątek, S. Afyon, T.M. Budnyak, S. Budnyk, M.H. Sipponen, A. Slabon, Sustainable Li-ion batteries: chemistry and recycling, Adv. Energy Mater. 11 (2021) 2003456, https://doi.org/10.1002/aenm.202003456.
[16] P. Wasserscheid, Transition Metal Catalysis in Ionic Liquids, Handb Green Chem, American Cancer Society, in, 2010, pp. 65–91, https://doi.org/10.1002/9783527628698.hgc062.
[17] A.J. Greer, J. Jacquemin, C. Hardacre, Industrial applications of ionic liquids, Molecules 25 (2020) 5207, https://doi.org/10.3390/molecules25215207.
[18] P.M. Dean, J.M. Pringle, D.R. MacFarlane, Structural analysis of low melting organic salts: perspectives on ionic liquids, Phys. Chem. Chem. Phys. 12 (2010) 9144–9153, https://doi.org/10.1039/C003519J.
[19] S. Zahn, F. Uhlig, J. Thar, C. Spickermann, B. Kirchner, Intermolecular forces in an ionic liquid ([Mmim][cl]) versus those in a typical salt (NaCl), Angew. Chem. Int. Ed. 47 (2008) 3639–3641, https://doi.org/10.1002/anie.200705526.
[20] T. Endo, K. Sunada, H. Sumida, Y. Kimura, Origin of low melting point of ionic liquids: dominant role of entropy, Chem. Sci. 13 (2022) 7560–7565, https://doi.org/10.1039/D2SC02342C.
[21] C.-W. Cho, T.P.T. Pham, Y. Zhao, S. Stolte, Y.-S. Yun, Review of the toxic effects of ionic liquids, Sci. Total Environ. 786 (2021) 147309, https://doi.org/10.1016/j.scitotenv.2021.147309.
[22] A.A. Quintana, A.M. Sztapka, V.C. Santos Ebinuma, C. Agatemor, Enabling sustainable chemistry with ionic liquids and deep eutectic solvents: a fad or the future? Angew. Chem. Int. Ed. 134 (2022) e202205609.
[23] P. Di Bernardo, A. Melchior, M. Tolazzi, P.L. Zanonato, Thermodynamics of lanthanide(III) complexation in non-aqueous solvents, Coord. Chem. Rev. 256 (2012) 328–351, https://doi.org/10.1016/j.ccr.2011.07.010.
[24] P. Di Bernardo, A. Melchior, R. Portanova, M. Tolazzi, P.L.L. Zanonato, Complex formation of N-donor ligands with group 11 monovalent ions, Coord. Chem. Rev. 252 (2008) 1270–1285, https://doi.org/10.1016/j.ccr.2007.12.007.
[25] A. Melchior, M. Sanadar, R. Cappai, M. Tolazzi, Entropy and enthalpy effects on metal complex formation in non-aqueous solvents: the case of silver(I) and monoamines, Entropy 24 (2022) 1253, https://doi.org/10.3390/e24091253.
[26] M. Sanadar, A. Kovačević, M. Cracchiolo, A. Melchior, M. Tolazzi, Thermodynamics of complex formation of silver(I) with substituted pyridines and cyclic amines in non-aqueous solvents, J. Therm. Anal. Calorim. (2024), https://doi.org/10.1007/s10973-024-12894-2.
[27] A. Melchior, M. Tolazzi, Thermodynamics of complex formation in dimethylsulfoxide: the case of co(II) complexes with nitrogen donor ligands and their O_2 adducts, Inorg. Chim. Acta 493 (2019) 91–101, https://doi.org/10.1016/j.ica.2019.04.010.
[28] L. Liu, G. Tian, L. Rao, Effect of solvation? Complexation of neodymium(III) with nitrate in an ionic liquid (BumimTf2N) in comparison with water, Solvent Extr. Ion Exch. 31 (2013) 384–400, https://doi.org/10.1080/07366299.2013.800410.
[29] A. Melchior, C. Gaillard, S. Gràcia Lanas, M. Tolazzi, I. Billard, S. Georg, L. Sarrasin, M. Boltoeva, Nickel(II) complexation with nitrate in dry [C_4mim][Tf_2N] ionic liquid: A spectroscopic, microcalorimetric, and molecular dynamics study, Inorg. Chem. 55 (2016) 3498–3507, https://doi.org/10.1021/acs.inorgchem.5b02937.
[30] T. Takamuku, Solvent properties of ionic liquids on complex formation of Ni(II) ion with molecular liquids, Anal. Sci. 41 (2025) 609–622, https://doi.org/10.1007/s44211-025-00741-9.
[31] M. Maseda, T. Takamuku, 1H, 13C, 15N NMR, and DFT studies on complex formation of zinc(II) ion with Ethylenediamine in ionic liquid [C2mIm][TFSA], J. Phys. Chem. B 128 (2024) 9500–9511, https://doi.org/10.1021/acs.jpcb.4c02590.
[32] S.A. Ansari, L. Liu, L. Rao, Binary lanthanide(III)/nitrate and ternary lanthanide (III)/nitrate/chloride complexes in an ionic liquid containing water: optical

absorption and luminescence studies, Dalton Trans. Camb. Engl. 2003 (44) (2015) 2907–2914, https://doi.org/10.1039/c4dt03479a.
[33] S.K. Singh, A.W. Savoy, Ionic liquids synthesis and applications: an overview, J. Mol. Liq. 297 (2020) 112038, https://doi.org/10.1016/j.molliq.2019.112038.
[34] F. Wu, F. Jiang, J. Yang, W. Dai, D. Lan, J. Shen, Z. Fang, Investigation of molecular mechanism of cobalt porphyrin catalyzed CO2 electrochemical reduction in ionic liquid by in-situ SERS, Molecules 28 (2023), https://doi.org/10.3390/molecules28062747.
[35] S.A. Satyawirawan, R.W. Cattrall, S.D. Kolev, M.I.G.S. Almeida, Improving co(II) separation from Ni(II) by solvent extraction using phosphonium-based ionic liquids, J. Mol. Liq. 380 (2023) 121764, https://doi.org/10.1016/j.molliq.2023.121764.
[36] S.A. Ansari, L. Liu, P.D. Dau, J.K. Gibson, L. Rao, Unusual complexation of nitrate with lanthanides in a wet ionic liquid: a new approach for aqueous separation of trivalent f-elements using an ionic liquid as solvent, RSC Adv. 4 (2014) 37988–37991, https://doi.org/10.1039/C4RA08252D.
[37] R.B. Gujar, S.A. Ansari, P. Sahoo, S.M. Ali, P.K. Mohapatra, Complexation thermodynamics of lanthanides with 2-thenoyltrifluoroacetone in a room temperature ionic liquid. Part-II: calorimetry and MD simulation studies, New J. Chem. 47 (2023) 868–874.
[38] L. Xu, N. Pu, G. Ye, C. Xu, J. Chen, X. Zhang, L. Lei, C. Xiao, Unraveling the complexation mechanism of actinide(III) and lanthanide(III) with a new tetradentate phenanthroline-derived phosphonate ligand, Inorg. Chem. Front. 7 (2020) 1726–1740, https://doi.org/10.1039/D0QI00200C.
[39] S.D. Chowta, A. Sengupta, G. Sugilal, P.K. Mohapatra, Ligand free extraction of tri-, tetra-, and hexa-valent actinide ions from aqueous hydrochloric acid medium using task specific ionic liquids, J. Mol. Liq. 427 (2025) 127324, https://doi.org/10.1016/j.molliq.2025.127324.
[40] T. Takamuku, in: K. Nishiyama, T. Yamaguchi, T. Takamuku, N. Yoshida (Eds.), Mixing States of Ionic Liquid-Molecular Liquid Mixed Solvents and their Effects on Metal Complex Formation BT - Molecular Basics of Liquids and Liquid-Based Materials, Springer Nature Singapore, Singapore, 2021, pp. 233–253, https://doi.org/10.1007/978-981-16-5395-7_8.
[41] G. Kaur, H. Kumar, M. Singla, Diverse applications of ionic liquids: A comprehensive review, J. Mol. Liq. 351 (2022) 118556, https://doi.org/10.1016/j.molliq.2022.118556.
[42] X. Wu, X. Li, L. Xu, W. He, Z. Zhou, W. Liu, F. Zhang, Z. Ren, Application of silver ionic liquid in the separation of olefin and alkane, J. Chem. Technol. Biotechnol. 97 (2022) 1207–1214, https://doi.org/10.1002/jctb.7009.
[43] M. Busato, A. Lapi, P. D'Angelo, A. Melchior, Coordination of the Co^{2+} and Ni^{2+} ions in Tf_2N^- based ionic liquids: A combined X-ray absorption and molecular dynamics study, J. Phys. Chem. B 125 (2021) 6639–6648, https://doi.org/10.1021/acs.jpcb.1c03395.
[44] M. Busato, P. D'Angelo, A. Melchior, Solvation of Zn^{2+} ion in 1-alkyl-3-methylimidazolium bis(trifluoromethylsulfonyl)imide ionic liquids: a molecular dynamics and X-ray absorption study, Phys. Chem. Chem. Phys. 21 (2019) 6958–6969.
[45] M. Busato, P. D'Angelo, A. Lapi, M. Tolazzi, A. Melchior, Solvation of Co^{2+} ion in 1-butyl-3-methylimidazolium bis(trifluoromethylsulfonyl)imide ionic liquid: A molecular dynamics and X-ray absorption study, J. Mol. Liq. 299 (2020) 112120, https://doi.org/10.1016/j.molliq.2019.112120.
[46] K. Fujii, T. Nonaka, Y. Akimoto, Y. Umebayashi, S. Ishiguro, Solvation structures of some transition metal(II) ions in a room-temperature ionic liquid, 1-Ethyl-3-methylimidazolium Bis(trifluoromethanesulfonyl)amide, Anal. Sci. 24 (2008) 1377–1380, https://doi.org/10.2116/analsci.24.1377.
[47] Y. Tsuchida, M. Matsumiya, K. Tsunashima, Solvation structure for Fe(II), co(II) and Ni(II) complexes in [P2225][NTf2] ionic liquids investigated by Raman spectroscopy and DFT calculation, J. Mol. Liq. 269 (2018) 8–13, https://doi.org/10.1016/j.molliq.2018.08.004.
[48] P. Nockemann, M. Pellens, K. Van Hecke, L. Van Meervelt, J. Wouters, B. Thijs, E. Vanecht, T.N. Parac-Vogt, H. Mehdi, S. Schaltin, J. Fransaer, S. Zahn, B. Kirchner, K. Binnemans, Cobalt(II) complexes of nitrile-functionalized ionic liquids, Chem. Eur. J. 16 (2010) 1849–1858.
[49] J. Sniekers, P. Geysens, T. Vander Hoogerstraete, L. Van Meervelt, J. Fransaer, K. Binnemans, Cobalt(II) liquid metal salts for high current density electrodeposition of cobalt, Dalton Trans. 47 (2018) 4975–4986, https://doi.org/10.1039/c8dt00283e.
[50] S. Schaltin, P. Nockemann, B. Thijs, K. Binnemans, J. Fransaer, Influence of the anion on the electrodeposition of cobalt from imidazolium ionic liquids, Electrochem. Solid-State Lett. 10 (2007) D104, https://doi.org/10.1149/1.2760185.
[51] J. Richter, T. Pietsch, M. Ruck, Cobalt deposition from Ionothermally dissolved cobalt oxides, ChemSusChem 16 (2023) e202300090, https://doi.org/10.1002/cssc.202300090.
[52] Y.-T. Hsieh, M.-C. Lai, H.-L. Huang, I.-W. Sun, Speciation of cobalt-chloride-based ionic liquids and electrodeposition of co wires, Electrochim. Acta 117 (2014) 217–223, https://doi.org/10.1016/j.electacta.2013.11.120.
[53] Y. Katayama, R. Fukui, T. Miura, Electrodeposition of Cobalt from an Imide-Type Room-Temperature Ionic Liquid, 2007, pp. 534–537, https://doi.org/10.1149/1.2768298.
[54] H.-W. Yeh, N. Serizawa, Y. Katayama, Electrochemical recovery of cobalt from cobalt oxide in an amide-type ionic liquid with low-temperature Carbochlorination, J. Electrochem. Soc. 168 (2021) 082502, https://doi.org/10.1149/1945-7111/ac180c.
[55] J.M. van Gaalen, J. Chris Slootweg, From critical raw materials to circular raw materials, ChemSusChem 18 (2025) e202401170, https://doi.org/10.1002/cssc.202401170.
[56] G. Alvial-Hein, H. Mahandra, A. Ghahreman, Separation and recovery of cobalt and nickel from end of life products via solvent extraction technique: a review, J. Clean. Prod. 297 (2021) 126592, https://doi.org/10.1016/j.jclepro.2021.126592.
[57] Q. Guo, Y. Chen, Z. Wu, Y. Liu, Y. Li, X. Du, M. Lin, Unveiling the mechanism of hydroxyl functional ionic liquid as co-extractant for efficient removal of cobalt ions from simulated radioactive wastewater, J. Mol. Liq. 409 (2024) 125539, https://doi.org/10.1016/j.molliq.2024.125539.
[58] F. Billeci, H.Q.N. Gunaratne, P. Licence, K.R. Seddon, N.V. Plechkova, F. D'Anna, Ionic liquids–cobalt(II) Thermochromic complexes: how the structure Tunability affects "self-contained" systems, ACS Sustain. Chem. Eng. 9 (2021) 4064–4075, https://doi.org/10.1021/acssuschemeng.0c08586.
[59] S. Belić, M. Vraneš, S. Papović, J. Magyari, M. Rodić, S. Gadžurić, Thermochromic behaviour and thermodynamics of cobalt(II) chloride complexes in ammonium nitrate + N-methylformamide mixture, J. Mol. Liq. (2019), https://doi.org/10.1016/j.molliq.2019.02.130.
[60] S. Tan, D. Zhang, Y. Chen, B.A. Helfrecht, E.T. Baxter, W. Cao, X.-B. Wang, M.-T. Nguyen, G.E. Johnson, V. Prabhakaran, Complexation of heavy metal cations with imidazolium ionic liquids lowers their reduction energy: implications for electrochemical separations, Green Chem. 26 (2024) 1566–1576, https://doi.org/10.1039/D3GC03713D.
[61] J.M. Hartley, C.M. Ip, G.C.H. Forrest, K. Singh, S.J. Gurman, K.S. Ryder, A. P. Abbott, G. Frisch, EXAFS study into the speciation of metal salts dissolved in ionic liquids and deep eutectic solvents, Inorg. Chem. 53 (2014) 6280–6288, https://doi.org/10.1021/ic500824r.
[62] N. Schaeffer, H. Passos, M. Gras, S.J. Rodriguez Vargas, M.C. Neves, L. Svecova, N. Papaiconomou, J.A.P. Coutinho, Selective separation of manganese, cobalt, and nickel in a fully aqueous system, ACS sustain, Chem. Eng. 8 (2020) 12260–12269.
[63] S. Georg, I. Billard, A. Ouadi, C. Gaillard, L. Petitjean, M. Picquet, V. Solov'ev, Determination of successive complexation constants in an ionic liquid: complexation of UO22+ with NO3− in C4-mimTf2N studied by UV−Vis spectroscopy, J. Phys. Chem. B 114 (2010) 4276–4282, https://doi.org/10.1021/jp9107624.
[64] C. Austen Angell, Y. Ansari, Z. Zhao, Ionic liquids: past, present and future, Faraday Discuss. 154 (2012) 9–27, https://doi.org/10.1039/C1FD00112D.
[65] K. Ueno, H. Tokuda, M. Watanabe, Ionicity in ionic liquids: correlation with ionic structure and physicochemical properties, Phys. Chem. Chem. Phys. 12 (2010) 1649–1658, https://doi.org/10.1039/B921462N.
[66] B. Kirchner, F. Malberg, D.S. Firaha, O. Hollóczki, Ion pairing in ionic liquids, J. Phys. Condens. Matter 27 (2015) 463002, https://doi.org/10.1088/0953-8984/27/46/463002.
[67] O. Hollóczki, F. Malberg, T. Welton, B. Kirchner, On the origin of ionicity in ionic liquids. Ion pairing versus charge transfer, Phys. Chem. Chem. Phys. 16 (2014) 16880–16890, https://doi.org/10.1039/C4CP01177E.
[68] O. Nordness, J.F. Brennecke, Ion dissociation in ionic liquids and ionic liquid solutions, Chem. Rev. 120 (2020) 12873–12902, https://doi.org/10.1021/acs.chemrev.0c00373.
[69] P. Gans, A. Sabatini, A. Vacca, Investigation of equilibria in solution. Determination of equilibrium constants with the HYPERQUAD suite of programs, Talanta 43 (1996) 1739–1753.
[70] P. Gans, A. Sabatini, A. Vacca, Determination of equilibrium constants from spectrophometric data obtained from solutions of known pH: the program pHab, Ann. Chim. 89 (1999) 45–49.
[71] J.-D. Chai, M. Head-Gordon, Long-range corrected hybrid density functionals with damped atom–atom dispersion corrections, Phys. Chem. Chem. Phys. 10 (2008) 6615–6620, https://doi.org/10.1039/B810189B.
[72] M.J. Frisch, G.W. Trucks, H.B. Schlegel, G.E. Scuseria, M.A. Robb, J.R. Cheeseman, G. Scalmani, V. Barone, G.A. Petersson, H. Nakatsuji, X. Li, M. Caricato, A. V. Marenich, J. Bloino, B.G. Janesko, R. Gomperts, B. Mennucci, H.P. Hratchian, J. V. Ortiz, A.F. Izmaylov, J.L. Sonnenberg, D. Williams-Young, F. Ding, F. Lipparini, F. Egidi, J. Goings, B. Peng, A. Petrone, T. Henderson, D. Ranasinghe, V. G. Zakrzewski, J. Gao, N. Rega, G. Zheng, W. Liang, M. Hada, M. Ehara, K. Toyota, R. Fukuda, J. Hasegawa, M. Ishida, T. Nakajima, Y. Honda, O. Kitao, H. Nakai, T. Vreven, K. Throssell, J.A. Montgomery Jr., J.E. Peralta, F. Ogliaro, M. J. Bearpark, J.J. Heyd, E.N. Brothers, K.N. Kudin, V.N. Staroverov, T.A. Keith, R. Kobayashi, J. Normand, K. Raghavachari, A.P. Rendell, J.C. Burant, S.S. Iyengar, J. Tomasi, M. Cossi, J.M. Millam, M. Klene, C. Adamo, R. Cammi, J.W. Ochterski, R.L. Martin, K. Morokuma, O. Farkas, J.B. Foresman, D.J. Fox, Gaussian 16, Rev. A.03, Gaussian 16 RevA03, Gaussian, Inc., Wallingford, CT, 2016.
[73] J.N. Canongia Lopes, J. Deschamps, A.A.H. Pádua, Modeling ionic liquids using a systematic all-atom force field, J. Phys. Chem. B 108 (2004) 2038–2047, https://doi.org/10.1021/jp0362133.
[74] J.N. Canongia Lopes, A.A.H. Padua, J. Dechamps, Additions and corrections, J. Phys. Chem. B 108 (2004) 11250, https://doi.org/10.1021/jp0476996.
[75] J.N. Canongia Lopes, A.A.H. Padua, Molecular force field for ionic liquids composed of Triflate or Bistriflyimide anions, J. Phys. Chem. B 108 (2004) 16893–16898, https://doi.org/10.1021/jp0476545.
[76] P. Li, B.P. Roberts, D.K. Chakravorty, K.M. Merz, Rational design of particle mesh ewald compatible lennard-jones parameters for +2 metal cations in explicit solvent, J. Chem. Theory Comput. 9 (2013) 2733–2748, https://doi.org/10.1021/ct400146w.
[77] B.H. Besler, K.M. Merz, P.A. Kollman, Atomic charges derived from semiempirical methods, J. Comput. Chem. 11 (1990) 431–439, https://doi.org/10.1002/jcc.540110404.
[78] A.V. Marenich, C.J. Cramer, D.G. Truhlar, Universal solvation model based on solute Electron density and on a continuum model of the solvent defined by the

bulk dielectric constant and atomic surface tensions, J. Phys. Chem. B 113 (2009) 6378–6396, https://doi.org/10.1021/jp810292n.
[79] R. Contreras, C.J. Cramer, D.G. Truhlar, V.S. Bernales, A.V. Marenich, Quantum mechanical continuum solvation models for ionic liquids, J. Phys. Chem. B 116 (2012) 9122–9129, https://doi.org/10.1021/jp304365v.
[80] M.J. Abraham, T. Murtola, R. Schulz, S. Páll, J.C. Smith, B. Hess, E. Lindah, Gromacs: high performance molecular simulations through multi-level parallelism from laptops to supercomputers, SoftwareX 1–2 (2015) 19–25, https://doi.org/10.1016/j.softx.2015.06.001.
[81] L. Chen, H.-H. Cui, S.E. Stavretis, S.C. Hunter, Y.-Q. Zhang, X.-T. Chen, Y.-C. Sun, Z. Wang, Y. Song, A.A. Podlesnyak, Z.-W. Ouyang, Z.-L. Xue, Slow magnetic relaxations in cobalt(II) Tetranitrate complexes. Studies of magnetic anisotropy by inelastic neutron scattering and high-frequency and high-field EPR spectroscopy, Inorg. Chem. 55 (2016) 12603–12617, https://doi.org/10.1021/acs.inorgchem.6b01544.
[82] A. Lewandowski, I. Stępniak, Relative molar Gibbs energies of cation transfer from a molecular liquid to ionic liquids at 298.15 K, Phys. Chem. Chem. Phys. 5 (2003) 4215–4218, https://doi.org/10.1039/B305734H.
[83] G.S. Tsebrikova, I.S. Ivanova, A.B. Ilyukhin, I.A. Yakushev, P.V. Dorovatovskii, V.P. Solov'ev, V.E. Baulin, A.Yu., Tsivadze, Co^{2+}, Ni^{2+} and Cu^{2+} complexes with phosphorylated derivatives of cyclen and diaza-18-crown-6: effect of anion on the structure of complexes and their stability in solution, Inorg. Chim. Acta 549 (2023) 121410, https://doi.org/10.1016/j.ica.2023.121410.
[84] W. Libus, L. Fraczyk, B. Chachulski, Properties and stability of $CoNO3^{+}$ complex in acetonitrile solution, Pol. J. Chem. 52 (1978) 493–498.
[85] A.E. Martell, R.D. Hancock, R.J. Motekaitis, Factors affecting stabilities of chelate, macrocyclic and macrobicyclic complexes in solution, Coord.Chem.Rev. 133 (1994) 39–65, https://doi.org/10.1016/0010-8545(94)80056-1.
[86] N. Banić, M. Vraneš, B. Abramović, J. Csanádi, S. Gadžurić, Thermochromism, stability and thermodynamics of cobalt(II) complexes in newly synthesized nitrate based ionic liquid and its photostability, Dalton Trans. 43 (2014) 15515–15525, https://doi.org/10.1039/c4dt01836b.
[87] S. Ishiguro, K. Ozutsumi, H. Ohtaki, Calorimetric and spectrophotometric studies of chloro complexes of manganese(II) and cobalt(II) ions in N,N-dimethylformamide, J. Chem. Soc. Faraday Trans. 1 Phys. Chem. Condens. Phases 84 (1988) 2409–2419, https://doi.org/10.1039/F19888402409.
[88] H. Suzuki, S. Ishiguro, H. Ohtaki, Formation of chloro complexes of manganese(II), cobalt(II), nickel(II) and zinc(II) in dimethyl sulphoxide, J. Chem. Soc. Faraday Trans. 86 (1990) 2179, https://doi.org/10.1039/ft9908602179.
[89] K. Fujii, Y. Umebayashi, R. Kanzaki, D. Kobayashi, R. Matsuura, S. Ishiguro, Thermodynamic aspects of metal–ion complexation in the structured solvent, N-methylformamide, J. Solut. Chem. 34 (2005) 739–753, https://doi.org/10.1007/s10953-005-5114-9.
[90] M.S. Lee, Y.J. Oh, Estimation of thermodynamic properties and ionic equilibria of cobalt chloride solution at 298 K, Mater. Trans. 45 (2004) 1317–1321, https://doi.org/10.2320/matertrans.45.1317.
[91] M. Uchikoshi, Determination of the distribution of cobalt-chloro complexes in hydrochloric acid solutions at 298 K, J. Solut. Chem. 47 (2018) 2021–2038.
[92] S. Sobekova Foltova, T. Vander Hoogerstraete, D. Banerjee, K. Binnemans, Samarium/cobalt separation by solvent extraction with undiluted quaternary ammonium ionic liquids, Sep. Purif. Technol. 210 (2019) 209–218.